Article

Current Biology

Sleep spindles promote hippocampal network downregulation during sleep

Graphical abstract

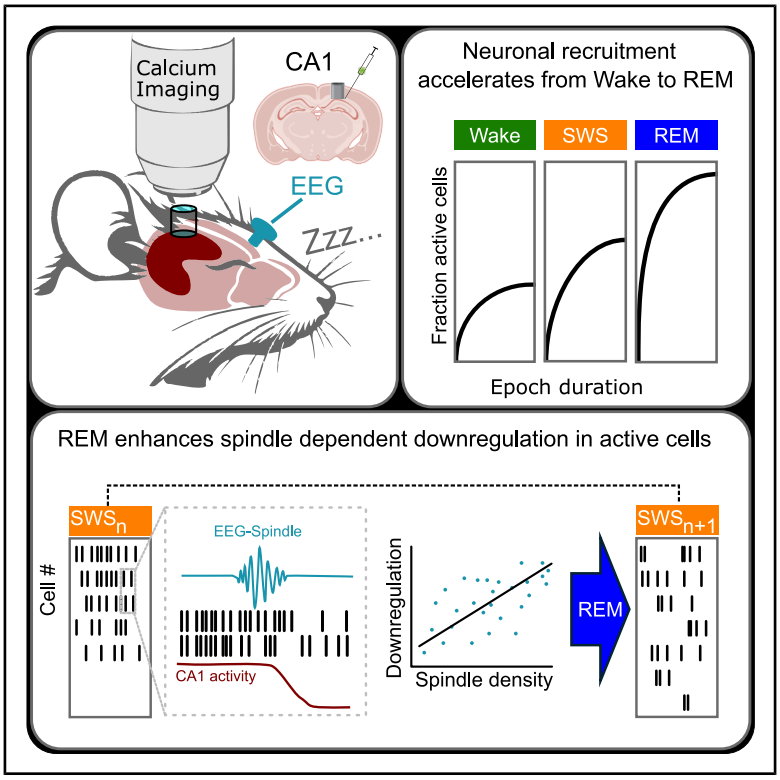

Authors

Niels Niethard, Diego Marco Pagano, Nima Mojtahedi, Yury Kovalchuk, Jan Born, Olga Garaschuk

Correspondence

olga.garaschuk@uni-tuebingen.de

In brief

Niethard et al. identify a mechanism for hippocampal renormalization during sleep where cortical spindles and REM sleep cooperate to drive the downregulation of CA1 neuronal activity. These findings reveal how sleep oscillations potentially support systems-memory consolidation.

Highlights

- CA1 active cell fractions rise from 28% in wake to 42% in SWS and 48% in REM sleep
- Spindle density predicts long-term downregulation of Ca^{2+} signaling in CA1
- Cortical spindles trigger an immediate decrease in CA1 neuronal signaling
- REM sleep enhances downregulation of CA1 cells active during SOs and spindles

Niethard et al., 2026, Current Biology *36*, 1385–1398
March 23, 2026
https://doi.org/10.1016/j.cub.2026.01.075

CellPress

Current Biology

CellPress
OPEN ACCESS

Article

Sleep spindles promote hippocampal network downregulation during sleep

Niels Niethard,[1,2,3,8] Diego Marco Pagano,[4,8] Nima Mojtahedi,[4] Yury Kovalchuk,[4] Jan Born,[1,3,5,6,7] and Olga Garaschuk[4,5,9,*]

[1]Institute of Medical Psychology and Behavioral Neurobiology, University of Tübingen, 72076 Tübingen, Germany
[2]Department of Cognitive Sciences, University of California, Irvine, Irvine, CA 92617, USA
[3]Institute for Diabetes Research and Metabolic Diseases of the Helmholtz Center Munich, University Tübingen (IDM), 72076 Tübingen, Germany
[4]Institute of Physiology, Department of Neurophysiology, University of Tübingen, 72074 Tübingen, Germany
[5]Center for Integrative Neuroscience, University of Tübingen, 72076 Tübingen, Germany
[6]German Center for Diabetes Research (DZD), 72076 Tübingen, Germany
[7]German Center for Mental Health (DZPG), 72076 Tübingen, Germany
[8]These authors contributed equally
[9]Lead contact
*Correspondence: olga.garaschuk@uni-tuebingen.de
https://doi.org/10.1016/j.cub.2026.01.075

SUMMARY

Sleep is thought to globally downregulate neuronal network activity and synaptic connections enhanced during prior wakefulness and, in parallel, to upregulate activity in networks mediating the consolidation of hippocampus-dependent episodic memory. To assess these processes in hippocampal networks during natural sleep, we combined the two-photon Ca^{2+} imaging of CA1 neuronal activity in mice with electroencephalogram (EEG) recordings of sleep slow oscillations (SOs) and spindles as markers of ongoing memory processing during slow-wave sleep (SWS). We found that the number of active hippocampal neurons increased from wakefulness into sleep, peaking during rapid eye movement (REM) sleep. At the population level, Ca^{2+} signaling did not decrease during individual SWS or REM epochs. Instead, we observed a gradual, persistent downregulation of Ca^{2+} signaling across consecutive SWS epochs, specifically in neurons active during the preceding SWS epoch. In cells active during SOs and spindles, this downregulation was particularly pronounced when the SWS epochs were separated by a REM sleep epoch. Sleep spindle density during the preceding SWS epoch was the strongest predictor of this across-epochs downregulation. Moreover, spindle onsets were followed (within 1 s) by an immediate reduction in both the fraction of active cells and their mean Ca^{2+} transient amplitude. Our findings point to a spindle-associated mechanism that, in cooperation with intermittent REM sleep, drives the progressive downregulation of hippocampal network activity across sleep, potentially supporting systems memory consolidation.

INTRODUCTION

Sleep is thought to play a 2-fold role in the regulation of the brain's network excitability and connectivity: (1) to help preserve or even strengthen synaptic connections, thereby supporting the formation of long-term memories, and (2) to globally downregulate synaptic connections formed in the process of information uptake during prior wakefulness and, thereby, protect networks from synaptic saturation and overexcitation.[1–4] Sleep has been proposed to support memory through a systems-level consolidation process that involves coordinated interactions between neocortical and hippocampal networks.[5–8] According to the active systems consolidation framework, this process is thought to be regulated by the coordinated occurrence of oscillatory events hallmarking the stage of slow wave sleep (SWS), i.e., the slow oscillations (SOs) primarily generated in neocortical networks, the 10–16 Hz spindles originating from the thalamus, and 180–250 Hz ripples, which, in hippocampal networks, tend to coalesce with sharp waves to form sharp wave-ripple complexes.[9–11] SOs are composed of periods of hyperpolarized neocortical networks producing synchronously reduced activity (i.e., down states) that interleave longer depolarizing phases (up states), alternating with frequencies of 0.1–2 Hz.[9,12] Spindles are generated in an interplay between GABAergic neurons within the thalamic nucleus reticularis and glutamatergic thalamocortical projection neurons. Spindle generation is driven by the depolarizing phase of the SO such that the spindles tend to nest into the SO up state.[9,13,14] Solitary spindles as well as spindles nesting in SO up states have been linked to the induction of synaptic plasticity and the upregulation of synaptic connections in neocortical networks.[15–17] Ripples accompany the memory replay of neuronal assembly firing patterns in hippocampal networks and themselves tend to nest into the excitable troughs of spindle oscillations, i.e., the phase of the oscillation where excitatory inputs to cortical neurons are strongly enhanced.[9,18–22] Spindles presumably reach the hippocampus

via the thalamic nucleus reuniens.[23] The triple nesting of SO-spindle-ripple events has been proposed as a core mechanism promoting the strengthening of memory representations in the neocortex during sleep-dependent system consolidation.[19–21]

Slow oscillatory activity as well as ripples might, at the same time, also play a role in downregulating synaptic connections during sleep in the neocortex and hippocampus.[4,24,25] Indeed, whereas the view—as proposed by the synaptic homeostasis hypothesis (SHY)—of a global downregulation of synaptic connectivity occurring across longer sleep periods has been supported by numerous studies using different functional and structural measures, it is currently less clear which of the different sleep stages (SWS or rapid eye movement [REM] sleep or both) and which oscillatory events associated with these sleep stages significantly contribute to the downregulation process.[26,27] Computational and experimental evidence supports a major contribution of SWS and slow oscillatory activity to synaptic downregulation in neocortical networks.[28–30] However, other work points to a contribution of REM sleep theta activity.[31,32] Using two-photon Ca^{2+} imaging of neocortical pyramidal cells, we observed a global decrease in activity of pyramidal cells across both SWS and REM sleep epochs, with the REM sleep-related decrease being more persistent than that during SWS.[33] Moreover, in this study, pyramidal cells with high activity during spindles, against the general decrease, increased activity during SWS epochs.

Against this backdrop of findings in neocortical networks, this study aimed at exploring whether comparable dynamics occurred during the sleep process in hippocampal networks. Using *in vivo* two-photon Ca^{2+} imaging in mice, we examined neuronal activity in the hippocampal CA1 region during unprovoked wakefulness, SWS, and REM sleep, as well as during SOs and spindles occurring in isolation or nesting in SO up states. For the neuronal population as a whole, we found that, in terms of the fraction of active neurons, overall neuronal activity increased during sleep in comparison with wakefulness and was largest during REM sleep. Contrasting with findings in the neocortex,[33] hippocampal Ca^{2+} signaling did not globally decrease during SWS or REM sleep epochs. But there was a downregulation of Ca^{2+} signaling across consecutive SWS epochs, which in neurons active during SOs and spindles was particularly pronounced when SWS epochs were interleaved by REM sleep. Downregulation of population activity was stronger the more spindles occurred during the preceding SWS epoch. Overall pointing to a cooperative action of spindles and REM sleep in downregulating hippocampal network activity.

RESULTS

Viral labeling of the CA1 area of the hippocampus with a genetically encoded Ca^{2+} indicator, GCaMP7b, enabled *in vivo* two-photon Ca^{2+} imaging of the CA1 pyramidal cell layer (excitatory/inhibitory neuron ratio $\sim$ 20:1; Figures S1A and S1B) in head-fixed mice (Figures 1A and 1B). Simultaneous electroencephalogram (EEG) and electromyogram (EMG) recordings allowed us to analyze how the activity of CA1 pyramidal neurons changed across cycles of wakefulness, SWS, and REM sleep (Figures 1C [STAR Methods] and S1–S5 for example data from all individual animals). Consistent with literature data from freely moving and head-fixed mice,[34,35] the animals that were extensively habituated to the experimental setup, on average, spent 49.6% of the recording time awake (mean epoch duration: 84.4 ± 6.19 s) and the remaining time sleeping (SWS, 42.5%, mean epoch duration, 63.61 ± 1.99 s; REM sleep, 7.9%, mean epoch duration, 84.52 ± 6.1 s; Figures 1D and 1E; $F = 5.7$, $p = 3.4 \times 10^{-3}$, permutation-based ANOVA followed by Tukey's post hoc test; Table S1). During wakefulness, the animals were typically quietly resting on the treadmill. They were free to move but were not engaged in any specific task or locomotor activities, as such stimulation would have interfered with the slowdown required for falling asleep. Thus, the wake periods preceding sleep bouts reflected a quiet resting state rather than active exploration or locomotion. All recording sessions started between 9 and 10 a.m. and lasted up to 5 h.

Throughout the study, we analyzed Ca^{2+} transient frequency as well as amplitude, as they capture distinct yet complementary aspects of neuronal dynamics. Frequency reflects the temporal pattern and recruitment of active cells across brain states, whereas amplitude more directly relates to the integrative strength of cellular activation and the magnitude of synaptic input.[36] Considering both dimensions can help to disentangle, e.g., whether state-dependent changes in hippocampal activity arise primarily from shifts in the number and timing of activation events or from altered activity patterns of individual cells within recruited ensembles.

Sleep increases the activity of CA1 pyramidal cells

Imaging the CA1 cell population at single-cell resolution, we found significant differences in the fractions of cells showing ongoing Ca^{2+} transients during different brain states (Figures 2A and 2B). Whereas only 28% of the total neuronal population was active during wake, the fraction of active cells increased during sleep, with 42% of cells active during SWS and 48% active during REM sleep (Figure 2B; $\chi^2 = 8.83$, $p = 0.01$). The mean frequency of Ca^{2+} transients in the active cells was lowest during SWS, intermediate during wake, and highest during REM sleep (Figure 2C, left; $\chi^2 = 15.86$, $p = 3.6 \times 10^{-4}$). The mean amplitude of the Ca^{2+} transients in active cells was also highest during REM sleep, intermediate during SWS, and lowest during wake (Figure 2C, right; $\chi^2 = 97.67$, $p < 6 \times 10^{-22}$), thus paralleling the pattern obtained for the fraction of active cells in each brain state (Figure 2B). For the entire population, i.e., including also inactive cells, the mean frequency of Ca^{2+} transients was the lowest during wake rather than SWS ($\chi^2 = 43.45$, $p < 4 \times 10^{-10}$; Figure 2D).

Next, we investigated the dynamics of cell recruitment during individual epochs of wakefulness, SWS, and REM sleep. In all brain states, the fraction of activated neurons tended to increase with increased duration of an epoch but at different rates (Figure 2E). Therefore, we normalized the epoch's length (setting it to 100%) and quantified the cell recruitment in the course of an epoch by calculating, for each epoch, the empirical cumulative distribution function (ECDF), providing the fraction of active neurons across each epoch in each brain state (Figures 2F and 2G). The analysis revealed that the recruitment is most gradual during wake epochs, intermediate during SWS, and steepest during

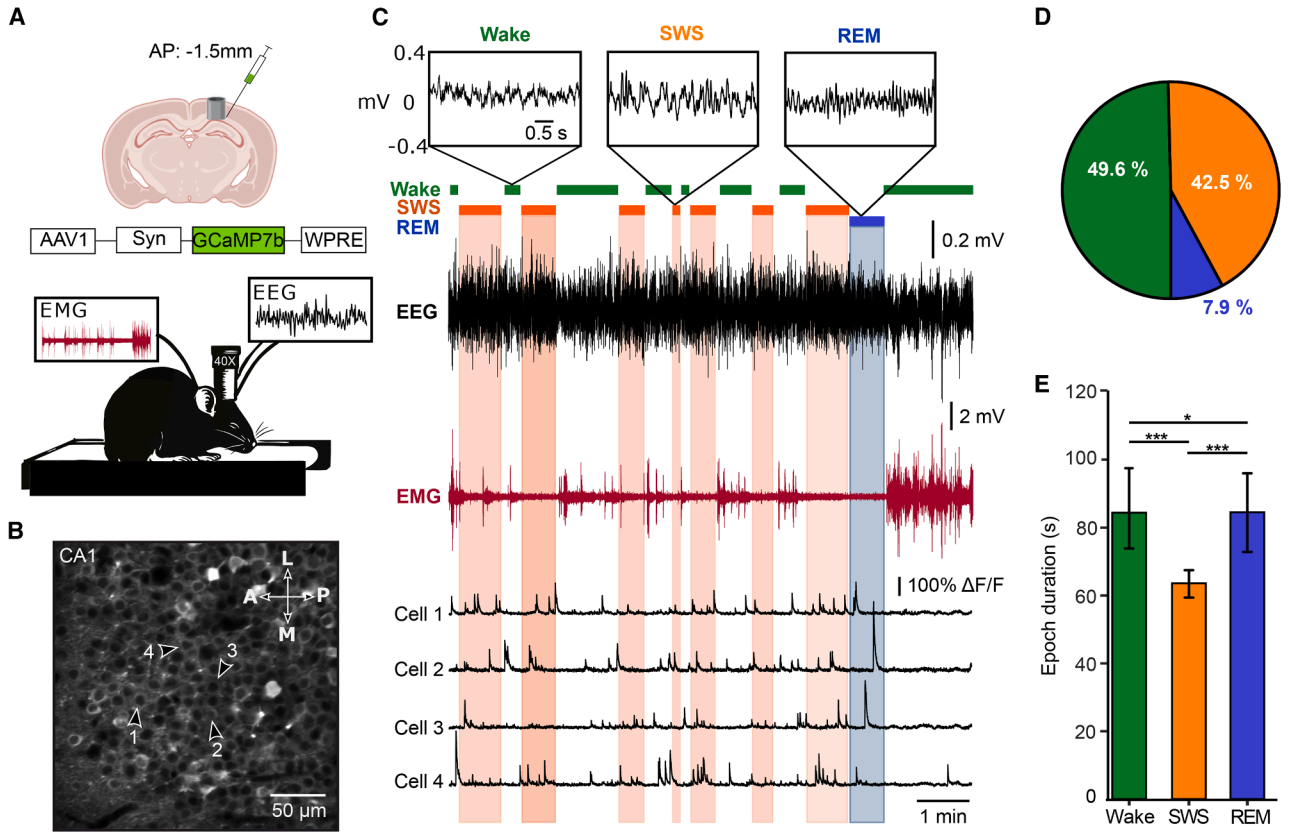

Figure 1. Brain state-specific activity in the CA1 area of the hippocampus

(A) The CA1 pyramidal cell layer of the dorsal hippocampus was injected with AAVs encoding GCaMP7b and sealed with the cranial window glued to a stainless-steel cannula (top). Besides the cranial window, EEG and nuchal muscle EMG electrodes were implanted (bottom). For recordings, the head-fixed mice were placed on a treadmill, and neuronal activity was recorded across wakefulness and spontaneous sleep.

(B) An image (average of 200 frames) of the CA1 pyramidal cell layer.

(C) A sample recording of wake (green), SWS (orange), and REM sleep (blue) epochs, along with the respective EEG (black) and EMG (red) traces. Inserts (top) show examples of the EEG traces recorded during wakefulness, SWS, and REM sleep, shown on an expanded timescale. Bottom traces (black) show corresponding Ca^{2+} signals from 4 representative pyramidal cells, marked with respective numbers in (B).

(D) Pie chart illustrating the fraction of recording time the animals spent in wake (green), SWS (orange), and REM (blue) states (35 h total, $n = 7$ mice).

(E) Bar graph illustrating mean bout durations of the three brain states ($n = 7$ mice, 856 wake, 854 SWS, and 114 REM epochs).

Data are shown as mean ± SEM. $^{*}p < 0.05$, $^{**}p < 0.01$, $^{***}p < 0.001$; permutation-based ANOVA followed by Tukey's post hoc test.

See also Figure S1 and Table S1.

REM sleep (Figure 2G; F = 391.8, $p < 2 \times 10^{-16}$, permutation-based ANOVA).

To check whether the recruitment of cells during different brain states occurs in a temporally grouped manner, we next quantified the fraction of coactive cells (i.e., cells showing Ca^{2+} transients within a 4-frame window). Windows with only one active cell were excluded. The fractions were comparable between wake and SWS but significantly lower during REM sleep ($\chi^2 = 8.63$, $p = 0.01$; Figure 2H). Additional analyses across epoch thirds revealed that co-activation remained stable within each state (data not shown). Finally, to assess how stable the activity patterns were across successive epochs, we compared the overlap between cell populations active in consecutive epochs (n and n + 1). The overlap was significantly lower during wakefulness compared with SWS and REM sleep ($\chi^2 = 22.63$, $p = 1 \times 10^{-5}$; Figure 2I), indicating that although wake activity involves relatively sparse yet synchronous activation of cells *within* epochs, the specific populations recruited across consecutive wake epochs vary more strongly than across consecutive epochs of SWS or REM sleep.

Mean frequency of the CA1 population Ca^{2+} signaling increases during wake epochs but remains stable over SWS and REM epochs

Following the idea that sleep is important for downregulating and renormalizing brain excitability, we investigated the dynamics of Ca^{2+} transients within wake, SWS, and REM sleep epochs, comparing the 1st, 2nd, and 3rd thirds of an epoch (Figures 2J and 2K). Looking at the total cell population, we observed a significant interaction between brain state and epoch thirds for the frequency of Ca^{2+} transients ($\chi^2 = 15.82$, $p = 0.003$; along with main effects of brain state, $\chi^2 = 120.90$, $p < 0.001$, and thirds, $\chi^2 = 22.50$, $p < 0.001$).

Direct comparisons between the 1st, 2nd, and 3rd thirds revealed that during wakefulness, the frequency of Ca^{2+} transients significantly increased from the 1st to the 2nd and 3rd thirds of an

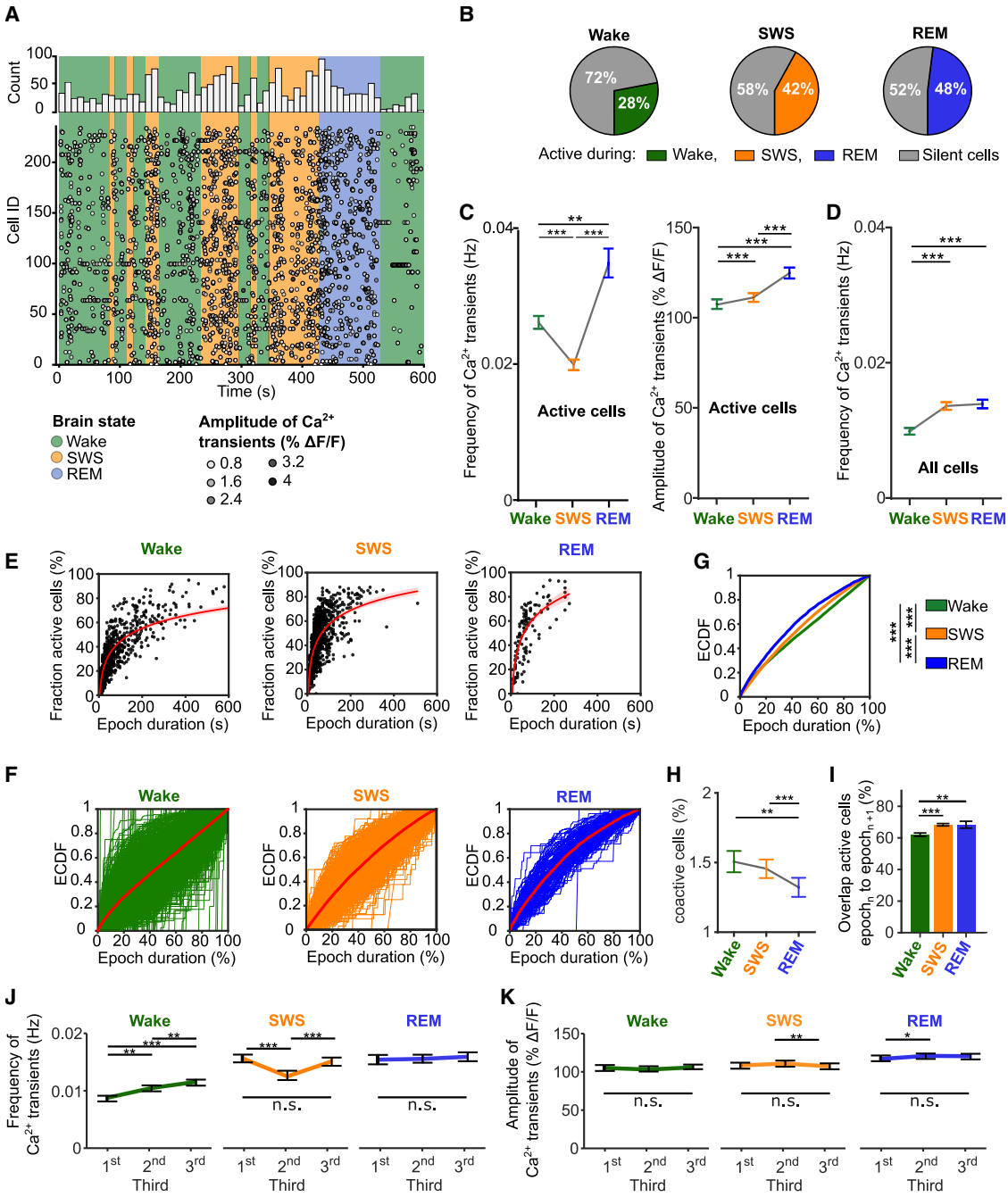

Figure 2. Distinct modulation of cellular activity across brain states

(A) Raster plot illustrating the activity of 236 CA1 pyramidal cells during a 10-min-long recording period. Individual ΔF/F traces of these cells are shown in Figure S5. Vertical stripes indicate the brain state: wake (green), SWS (orange), and REM (blue). Each dot represents a Ca^{2+} transient whose amplitude is color-coded using a grayscale. A histogram (top) gives the cumulative number of active cells in each 10-s-long bin.

(B) Pie charts, illustrating the fractions of active and silent pyramidal cells for each brain state (n = 1,335 cells from 7 mice). The distributions differ significantly between the 3 brain states (chi-square test, $\chi^2 = 8.83$, $p = 0.01$).

(C) Mean ± SEM frequency (left) and amplitude (right) of Ca^{2+} transients across consecutive wake, SWS, and REM epochs, only considering cells that showed at least one transient in the respective epoch (n = 7 mice, n = 108 epochs for each state), $^{**}p < 0.01$, $^{***}p < 0.001$; linear mixed model (LMM) followed by the Wilcoxon signed rank test.

(D) Mean ± SEM frequency of Ca^{2+} transients of all recorded cells in the different brain states (n = 7 mice, n = 108 epochs for each state). $^{**}p < 0.01$, $^{***}p < 0.001$; LMM followed by the Wilcoxon signed-rank test.

(E) Scatterplots showing the fraction of cells active during a given epoch as a function of epoch duration across wake, SWS, and REM sleep. Red lines show the kernel density estimations for the scatterplots (n = 856 wake, 854 SWS, and 114 REM epochs).

(legend continued on next page)

epoch. By contrast, during SWS, frequency was significantly decreased during the 2nd third compared with both the 1st and 3rd thirds (Figure 2J). No significant changes were observed across the thirds of a REM sleep epoch. In terms of amplitude, Ca^{2+} transients remained stable across the thirds of individual epochs in all three states ($p = 0.79$ for the main effect of thirds; Figure 2K).

Next, we compared Ca^{2+} signaling across two consecutive SWS epochs, separated by either a wake or a REM epoch, resulting in SWS_n-wake-SWS_{n+1} and SWS_n-REM-SWS_{n+1} triplets. Ca^{2+} transient frequency (Figures 3A and 3B) remained stable between SWS_n and SWS_{n+1} ($p > 0.18$ for respective pairwise comparisons) regardless of the intervening state. Due to the different transient frequency during wake and REM, the interaction between the intervening state and triplet position was significant in this analysis ($\chi^2 = 19.24$, $p < 0.001$). Similarly, Ca^{2+} transient amplitude (Figures S6A and S6B) also remained stable between epochs ($p > 0.09$ for the respective pairwise comparison and for the interaction effect between the intervening state and triplet position, $\chi^2 = 19.08$, $p < 0.001$).

Spindle density as a strong correlate of hippocampal renormalization

Given the central role SOs and spindles during SWS play for sleep-dependent plasticity, we correlated changes in the frequency of Ca^{2+} transients from SWS_n to SWS_{n+1} with the density of solitary SOs ("SO"), solitary spindles ("Spindles"), and coupled "SO + Spindle" events where spindles occurred during the SO up state (Table S2). Spindle density during the preceding SWS_n epoch emerged as the strongest negative predictor of changes in Ca^{2+} transient frequency across both REM- and wake-interleaved SWS pairs, i.e., when spindle density was high during the initial SWS_n epoch, Ca^{2+} transient frequency likely decreased across the two consecutive SWS epochs (Figures 3C and 3D; REM, $r = -0.30$, $p < 0.001$; wake, $r = -0.38$, $p < 0.001$). Similarly, SO + Spindle event density was negatively correlated with frequency changes, regardless of the interleaving state (REM, $r = -0.32$, $p < 0.001$; wake, $r = -0.24$, $p = 0.01$). By contrast, the density of solitary SOs was not significantly associated with frequency changes ($p > 0.06$). Interestingly, the duration of the initial SWS_n epoch was positively correlated with the change in Ca^{2+} transient frequency between SWS_n and SWS_{n+1}, indicating that SWS_n epochs of longer duration were more likely followed by an increase rather than a decrease in transient frequency in the SWS_{n+1} epoch (REM, $r = 0.28$, $p < 0.001$; wake, $r = 0.25$, $p = 0.01$).

SOs are known to increase in density after prolonged wake and thus serve as a marker of sleep pressure that decreases with time asleep (e.g., Vyazovskiy et al.[37]). Therefore, separately for data analyzed in Figures 3C and 3D, we examined correlations between the time of onset relative to the start of the recording session and the duration of SWS epochs, on the one hand, and the density of Spindle, SO, and SO + Spindle events, on the other hand. The time of SWS epoch onset was positively correlated with spindle density ($r = +0.30$, $p < 0.001$), whereas SWS epoch duration was negatively correlated with spindle density ($r = -0.27$, $p < 0.001$) but only for SWS epochs preceding interleaving wake epochs and not for those preceding REM sleep. No other event densities were associated with the time of SWS epoch onset or duration, overall ruling out that the observed correlations between activity dynamics across two consecutive SWS epochs and event densities were driven by epoch duration or onset.

Together, these findings suggest that neither individual SWS nor REM sleep epochs are consistently linked to lasting reductions in hippocampal CA1 pyramidal cell activity. Instead, spindle density emerges as the strongest correlate of hippocampal renormalization of activity across consecutive SWS epochs.

Cortical spindles are followed by a decrease in hippocampal Ca^{2+} signaling

To investigate the role of SOs, spindles, and coupled SO-spindles on Ca^{2+} signaling in the hippocampal CA1 area with higher temporal precision, we analyzed changes in neuronal activity within a ±3 s window around each event (using the −3 to −2 s interval as baseline). We first examined the baseline-corrected fraction of active cells per imaging frame, time-locked to the negative half-wave peak of the SO and the onset of spindles, respectively. There were no significant changes in the fraction of active cells linked to solitary SOs during the ±3 s window (Figure 4A, left). However, onsets of solitary spindles were followed by a distinct and persistent decrease in the fraction of active cells per frame between +1 and +3 s (Figure 4A, middle). SO + Spindle events were linked to a transient decrease in the fraction of active cells per frame shortly before the negative half-wave peak but otherwise did not elicit any significant modulation in the fraction of active cells (Figure 4A, right). To assess overall recruitment during these events, we averaged the fraction of active cells across the entire duration of an SO upstate and of spindle events, respectively. This analysis revealed greater cell recruitment during spindles compared with solitary SOs ($\chi^2 = 42.93$, $p < 0.001$). Importantly, this effect was present regardless of whether spindles occurred in isolation or were coupled to SOs (Figure 4C).

We also quantified the mean amplitude of Ca^{2+} transients across active cells for each frame within the ±3 s window around

(F) Brain-state-specific empirical cumulative distribution functions (ECDFs), illustrating for each epoch (with duration set to 100%) the temporal evolution of cells contributing to the network activity.
(G) The averaged ECDF vectors for the three brain states (***$p < 0.001$; permutation-based ANOVA followed by Tukey's post hoc test).
(H) Mean ± SEM fraction of coactive cells within each 133-ms-long (4 frames) time window across consecutive wake, SWS, and REM epochs. Coactivity was only considered when at least two cells were active simultaneously ($n = 7$ mice, $n = 108$ epochs per state), **$p < 0.01$, ***$p < 0.001$; the Friedman test was followed by the Wilcoxon signed-rank test.
(I) Mean ± SEM overlap of active cells between doublets of consecutive epochs ($epoch_n$ and $epoch_{n+1}$) of wake (green), SWS (orange), and REM sleep (blue). $n = 7$ mice; epoch doublets for wake, $n = 315$; SWS, $n = 410$; and REM, $n = 68$; *$p < 0.01$, ***$p < 0.001$, Kruskal-Wallis test followed by the Wilcoxon rank-sum test.
(J and K) Mean ± SEM frequency (J) and amplitude (K) of Ca^{2+} transients within the 1st, 2nd, and 3rd thirds of epochs of wake (left), SWS (middle), and REM (right) sleep ($n = 7$ mice, $n = 108$ epochs for each state). *$p \leq 0.05$, **$p < 0.01$, ***$p < 0.001$, LMM followed by the Wilcoxon signed-rank test.
See also Figures S2–S5.

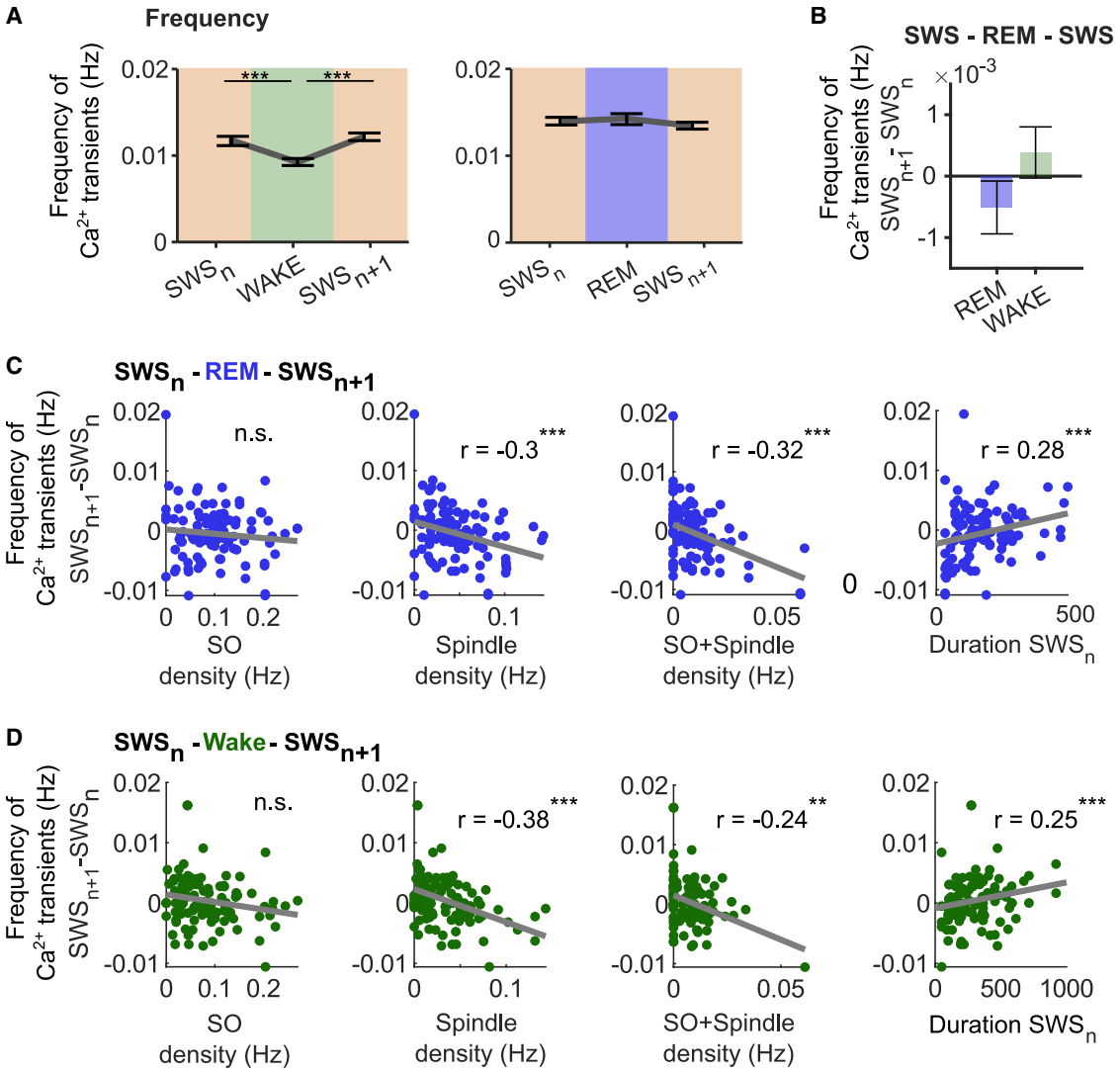

Figure 3. Frequencies of Ca^{2+} transients in the total cell population are stable across consecutive SWS epochs

(A) Mean ± SEM frequencies of Ca^{2+} transients during two consecutive epochs of SWS (SWS_n and SWS_{n+1}) interleaved by either a wake (left, n = 106 triplets) or REM sleep (right, n = 106 triplets) epoch. ***$p < 0.001$; LMM followed by the Wilcoxon signed-rank test.

(B) Mean ± SEM differences in frequency of Ca^{2+} transients between SWS_{n+1} and SWS_n. Wilcoxon rank-sum test.

(C and D) Scatterplots showing the relationship between the density of SOs, Spindles, and SO + Spindles and the duration of SWS_n epochs (x axis) and the difference in Ca^{2+} transient frequency in the first SWS_n and second SWS_{n+1} epoch, indicating the degree of downregulation across SWS_n-REM-SWS_{n+1} (C) and SWS_n-wake-SWS_{n+1} (D) triplets (y axis). Note that Spindle and SO + Spindle densities are predictive for a downregulation from SWS_n to SWS_{n+1} epochs. By contrast, SWS_n epoch durations positively correlate with changes from SWS_n to SWS_{n+1} epochs. Spearman correlation, *$p < 0.05$, **$p < 0.01$, ***$p < 0.001$. See also Tables S1 and S2.

the events of interest. This analysis revealed a pattern similar to that observed for active cell recruitment. Thus, solitary spindles were followed within 1 s after spindle onset by a pronounced decrease in mean Ca^{2+} transient amplitude (Figure 4B). Nevertheless, the mean amplitude of Ca^{2+} transients during the entire spindle event was still higher than during the up state of solitary SOs ($\chi^2 = 53.78$, $p < 0.001$; Figure 4D). Together, these findings support an association between spindles and the downregulation of hippocampal activity during sleep. Although when focusing on individual events, the magnitude of this modulation appears to be modest, these event-locked analyses revealed a robust and significant change, suggesting that spindles actively suppress hippocampal activity not only across extended SWS epochs but also at the level of individual events, with potential implications for memory consolidation.

Ca^{2+} transient amplitudes of cells active during SO and spindle events increase during REM epochs

Assuming that the activity of neurons during SOs, spindles, and combined SO-spindle events is related to memory processing, we examined whether cells particularly active during these events showed specific temporal dynamics within SWS epochs as well as across cycles of wake, SWS, and REM sleep. For determining subpopulations of SO-active, Spindle-active, and

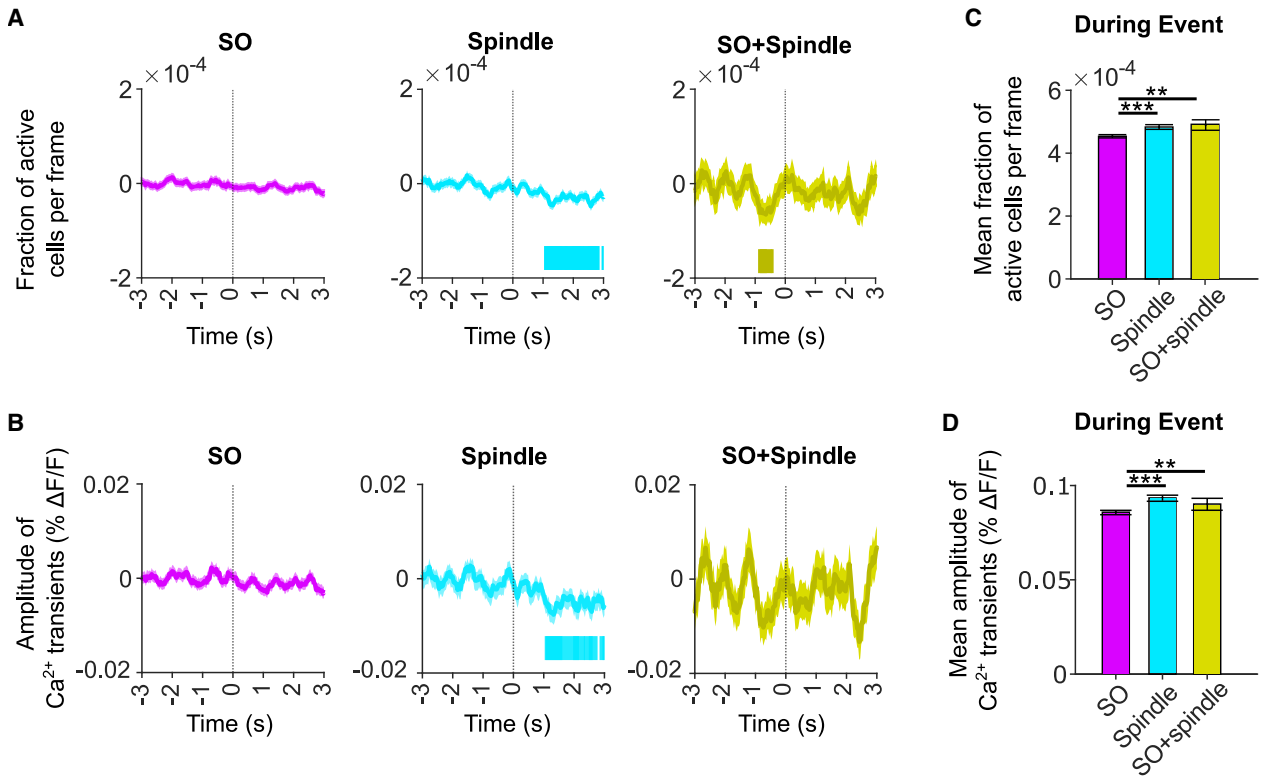

Figure 4. Spindle events are followed by a decreased fraction of active cells and lower mean Ca^{2+} transient amplitude

(A and B) Baseline-corrected (−3 to −2 s) mean ± SEM fraction of active cells per frame (A) and mean ± SEM amplitude of Ca^{2+} transients across all cells (B) time-locked to the negative half-wave peak of detected SOs (left, n = 9,498), spindle onset of solitary spindles (middle, n = 4,050), and spindle onset of SO + Spindles (right, n = 900). The time periods during which the differences from baseline levels are significant are marked by bars below the respective curves.

(C and D) Mean ± SEM fraction of active cells per frame (C) and mean ± SEM amplitude of Ca^{2+} transients across all active cells (D) during the SO up state or during spindle events (Spindles and SO + Spindles). $^{**}p < 0.01$, $^{***}p < 0.001$, Kruskal-Wallis test.

See also Table S2.

SO + Spindle-active cells, respectively, we first calculated for each cell the difference in the mean frequency of Ca^{2+} transients during the respective target events and during the remaining time of the respective SWS epoch (STAR Methods).[33] All cells with a positive difference were then defined as SO-active, Spindle-active, and SO + Spindle-active cells, respectively. Note, active cells were separately determined for each SWS epoch, and SO + Spindle-active cells did not count into the subpopulation of SO or spindle-active cells. The active cell populations were compared with a control population composed of those cells that did not meet the criteria for any of the three event-related subpopulations and exhibited at least one Ca^{2+} transient during the epoch.

We first compared the activity levels of SO-active, Spindle-active, and SO + Spindle-active cells with those of the control cell population during the current SWS epoch as well as during the preceding wake and subsequent REM sleep epochs. All four cell populations, SO-active, Spindel-active, SO + Spindle-active, and control cells, showed their highest Ca^{2+} transient frequencies during SWS compared with wake and REM sleep (Figures 5A and 5B; main effect of state: $\chi^2 = 89.98$, $p < 0.001$). As expected, during the SWS epochs, transient frequencies were generally higher in the three active cell subpopulations (SO-active, Spindle-active, and SO + Spindle active) than in the control population (all $p < 0.001$), and the same difference was observed for the preceding wake and succeeding REM sleep epochs (all $p < 0.001$, $\chi^2 = 85.55$, $p < 0.001$, for the main effect of subpopulation). However, the three kinds of active subpopulations did not significantly differ in Ca^{2+} transient frequency levels during any brain state (all $p > 0.15$; Figure 5B). In terms of Ca^{2+} transient amplitudes, all four subpopulations exhibited patterns similar to the overall population (Figures 2C and 2D), with the lowest amplitudes during wakefulness, intermediate amplitudes during SWS, and the highest amplitudes during REM sleep (main effect of brain state, $\chi^2 = 92.12$, $p < 0.001$; Figure 5C). Notably, amplitudes during the SWS epochs were highly comparable between the subpopulations (all $p > 0.69$). In the succeeding REM sleep epochs, Ca^{2+} transient amplitude decreased in the SO + Spindle-active cells, with this decrease reaching significance in comparison with SO-active cells ($p = 0.04$, $\chi^2 = 11.07$, $p = 0.09$ for interaction between subpopulation and brain state; Figure 5C).

We additionally compared the dynamics of Ca^{2+} transients for SO-, Spindle-, and SO + Spindle-active cells with that of control cells within individual epochs, i.e., across the 1st, 2nd, and 3rd thirds of SWS and neighboring wake and REM sleep epochs (Figures 6A and 6B). As to the frequency of Ca^{2+} transients, within-epoch dynamics for all 4 subpopulations were similar to

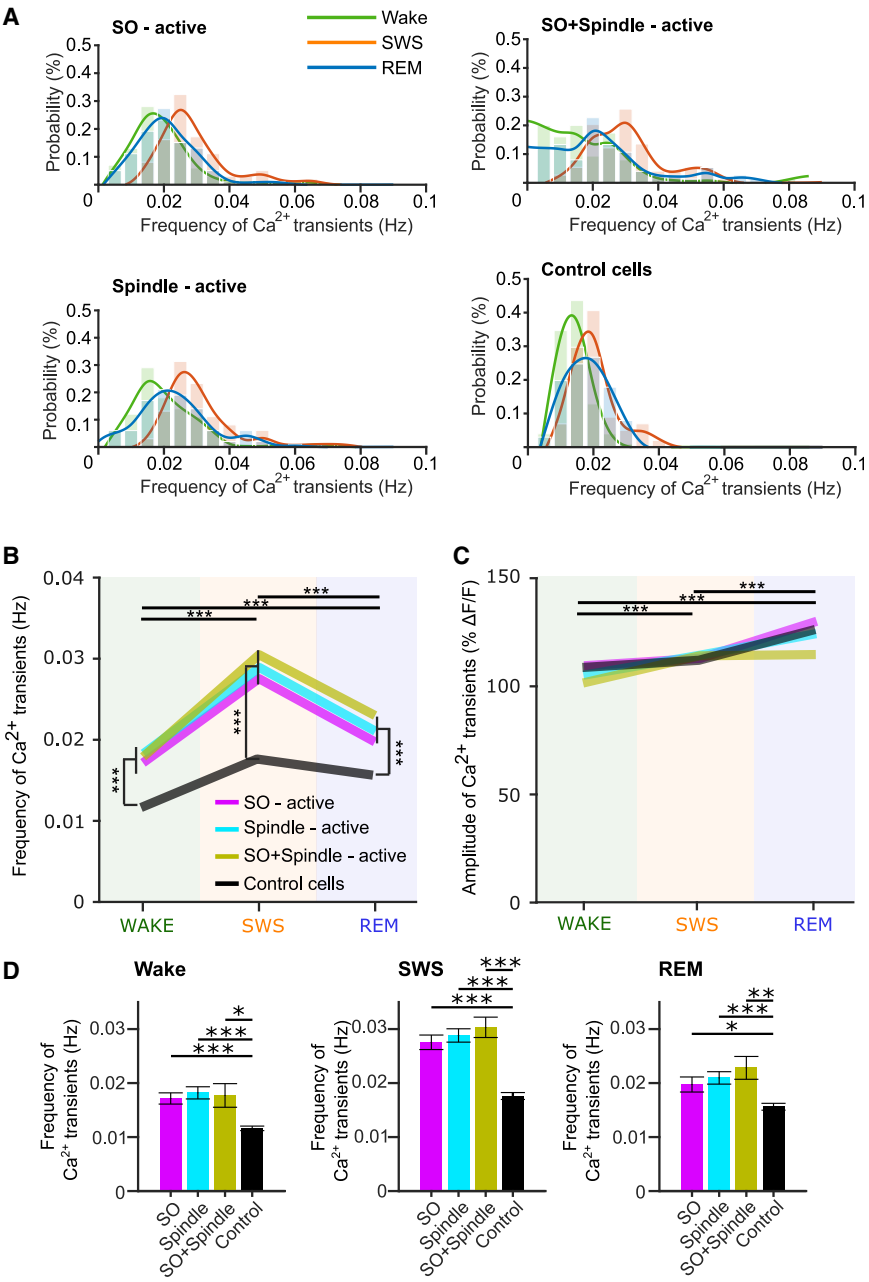

Figure 5. Activity levels of SO-active, Spindle-active, and SO + Spindle-active cells across consecutive wake, SWS, and REM sleep epochs

(A) Normalized histograms showing mean (per epoch) frequency of Ca^{2+} transients for SO-active (left top, n = 100 epochs), spindle-active (left bottom, n = 100 epochs), SO + Spindle-active (right top, n = 76 epochs), and (nonspecifically active) control cells (right bottom, n = 100 epochs) during consecutive wake (green), SWS (orange), and REM (blue) sleep epochs. The y axis shows the probability of observing a given Ca^{2+} transient frequency within each cell population for a given state, and the x axis indicates the transient frequency. Values were normalized to the total number of cells in each cluster, allowing direct comparison across states while accounting for differences in population size. Histograms are half transparent to visualize the smoothed fit to the respective histogram.

(B and C) Mean (per epoch) frequency (B) and amplitude (C) of Ca^{2+} transients for the consecutive wake, SWS, and REM sleep epochs (***p < 0.001; LMM followed by the Wilcoxon signed-rank test). For the analyses, cells active during an oscillatory event during SWS were tracked during the wake epoch preceding and the REM epoch following a specific SWS epoch.

(D) Mean ± SEM frequencies of Ca^{2+} transients for the consecutive wake, SWS, and REM sleep epochs of SO-, Spindle-, SO + Spindle-active, and control cells as shown in (B) (*p < 0.05, **p < 0.01, ***p < 0.001; LMM followed by the Wilcoxon signed-rank test).

those observed for the total population (Figure 2), i.e., Ca^{2+} transient frequency increased from the 1st to the 3rd third during wake (p < 0.04) but remained stable during SWS and REM sleep epochs (p > 0.06, χ^2 = 25.16, p < 0.001 for interaction between brain state and third; Figure 6A). This pattern also did not differ between the active subpopulations and the control population (Figure 6C). Changes in Ca^{2+} transient amplitudes within epochs appeared to be rather variable, with slightly increased amplitudes toward the 3rd third in wake epochs (χ^2 = 15.49, p < 0.001, main effect of third) and REM sleep (χ^2 = 7.07, p = 0.03, main effect of third). During REM sleep epochs, this increase was also significant for SO-active cells and for the combined subpopulation of SO-, Spindle-, and SO + Spindle-active cells when compared with the non-active control cell population showing no systematic change in amplitude (p = 0.03; Figure 6D). Examining the parallel dynamics of SO, spindle, and SO + Spindle event densities across the thirds of SWS epochs, we consistently observed the lowest event densities during the 2nd third (Figure S6C), closely resembling the overall dynamics observed across all cell clusters and the total cell population (Figure 2J).

In sum, while SO-, Spindle-, and SO + Spindle-active cells show distinctly enhanced activity across all brain states in comparison with control cells, these active subpopulations did not exhibit clear changes in their within-epochs dynamics, except for an overall tendency of increased transient amplitudes toward the 3rd third of REM epochs.

REM sleep-related downregulation is more pronounced for cells active during SO and spindles

Based on evidence from neocortical recordings that REM sleep may spare from downregulation circuits that are involved in memory formation,[32] and on our finding that spindles are accompanied by an immediate reduction in hippocampal Ca^{2+} transients (Figure 4), we examined how activity of SO-active, spindle-active, and SO + Spindle-active cells evolved across

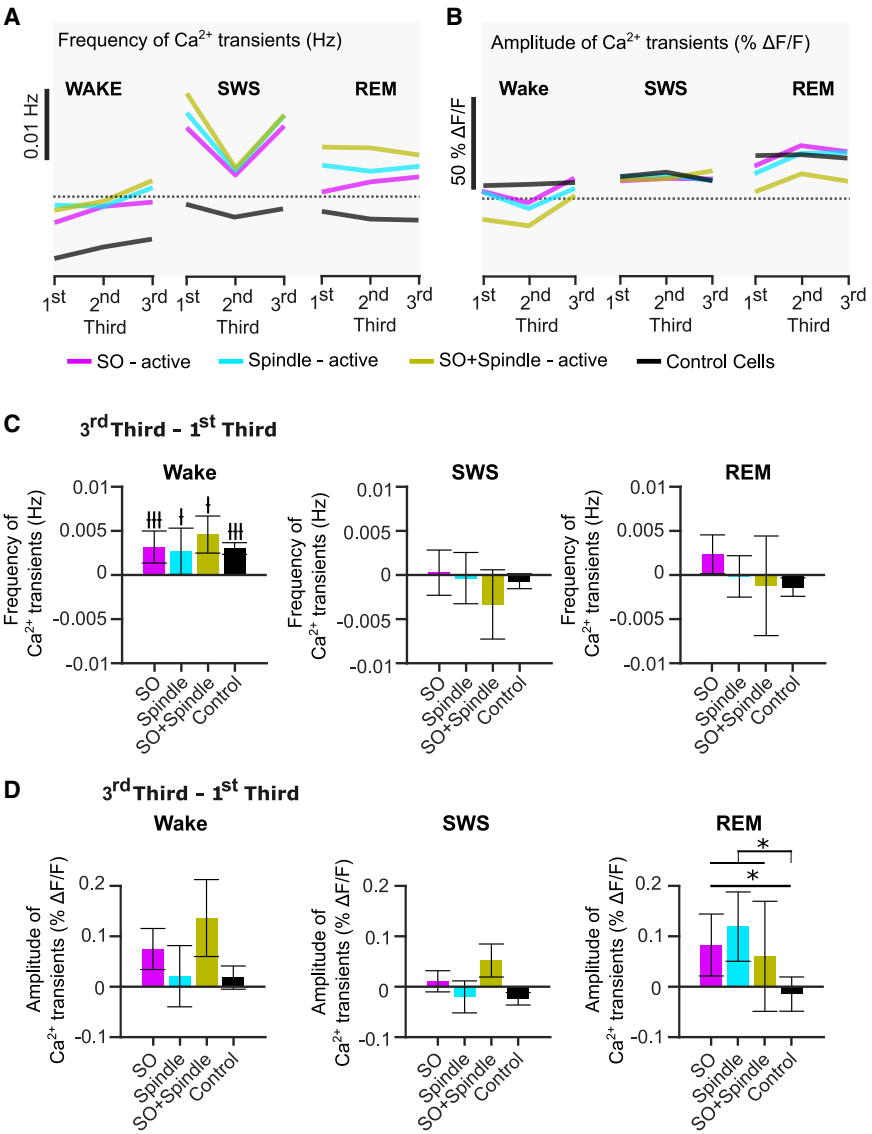

Figure 6. Ca^{2+} transient amplitudes of cells active during SOs increase across REM sleep epochs

(A and B) Mean Ca^{2+} transient frequencies (A) and amplitudes (B) of SO-active (n = 100 epochs per stage), spindle-active (n = 100 epochs per stage), SO + Spindle-active (n = 76 epochs per stage), and control cells (n = 100 epochs per stage) within the 1st, 2nd, and 3rd thirds of epochs of wake (left), SWS (middle), and REM sleep (right). Dashed lines indicate 0.02 Hz (A) and 100% ΔF/F (B).

(C and D) Mean ± SEM differences in Ca^{2+} transient frequency (C) and amplitudes (D) between the 1st and the 3rd third of wake (left), SWS (middle), and REM epochs (right). LMM followed by the Wilcoxon signed-rank test, $^{i}p < 0.05$, $^{iii}p < 0.001$, and the Mann-Whitney U test. $^{*}p < 0.05$. Additional comparison using the Mann-Whitney U test between merged SO, Spindle, and SO + Spindle subpopulations is indicated on top.

See also Figure S6.

DISCUSSION

We performed *in vivo* two-photon Ca^{2+} imaging of the CA1 area of the mouse hippocampus to investigate the dynamics of Ca^{2+} transients during wakefulness, SWS, and REM sleep. Our analyses addressed two main questions: (1) referring to the SHY,[4] we examined to what extent SWS and REM sleep contribute to a widespread downregulation of Ca^{2+} signaling in CA1 pyramidal cell networks, and these analyses concentrated on the dynamics of the total cell population. (2) Based on evidence for a central role of sleep in actively consolidating memory in the hippocampus-dependent episodic memory system,[2,7] we examined to what extent sleep leads to signs of upregulated Ca^{2+} signaling specifically in cell networks assumed to be involved in memory processing. For these analyses, we concentrated on the dynamics of cell subpopulations with distinctly enhanced activity during SOs, spindles, and SO-spindle events, i.e., oscillatory phenomena known to be involved in sleep-dependent memory formation. The main findings of our study are (1) the number of active cells in the total population of CA1 pyramidal cells increased from wakefulness to sleep, reaching a maximum during REM sleep. (2) Unexpectedly, we did not find, for the total population, signs of a global downregulation of Ca^{2+} signaling within SWS or REM sleep epochs or across consecutive SWS epochs. (3) Instead, we observed a specific decrease in hippocampal Ca^{2+} signaling across consecutive SWS epochs for active cells only. This downregulation was most pronounced in cells that, during the initial SWS epoch, were active during SO + Spindles, and when the SWS epochs were separated by a REM rather than a wake epoch. The gradual downregulation across SWS epochs was, moreover, strongly associated with spindle density in the preceding SWS epochs.

successive SWS epochs that were interleaved by either REM sleep (SWS_n-REM-SWS_{n+1} triplets) or wakefulness (SWS_n-wake-SWS_{n+1} triplets). The complementary analysis for the total cell population is shown in Figure 3. We found that all three active subpopulations, as well as the control cell population, exhibited significant reductions in Ca^{2+} transient frequency from SWS_n to SWS_{n+1}, regardless of whether the intervening state was REM sleep or wakefulness (Figure 7; $p < 0.01$ for all comparisons). However, the reduction following REM sleep was distinctly less pronounced in the control cells than in the SO-active, Spindle-active, and SO + Spindle-active cell populations ($\chi^2 = 11.42$, $p = 0.009$, main effect of subpopulation; Figure 7D). This pattern suggests that the lack of downregulation observed in the overall cell population (Figures 3A and 3B) may reflect the recruitment of new, previously inactive cells during SWS_{n+1}, while cells that are active during SWS_n undergo downregulation. The same analyses performed on the amplitudes of Ca^{2+} transients did not reveal any significant modulation across both types of triplets ($p \geq 0.17$; Figure S7).

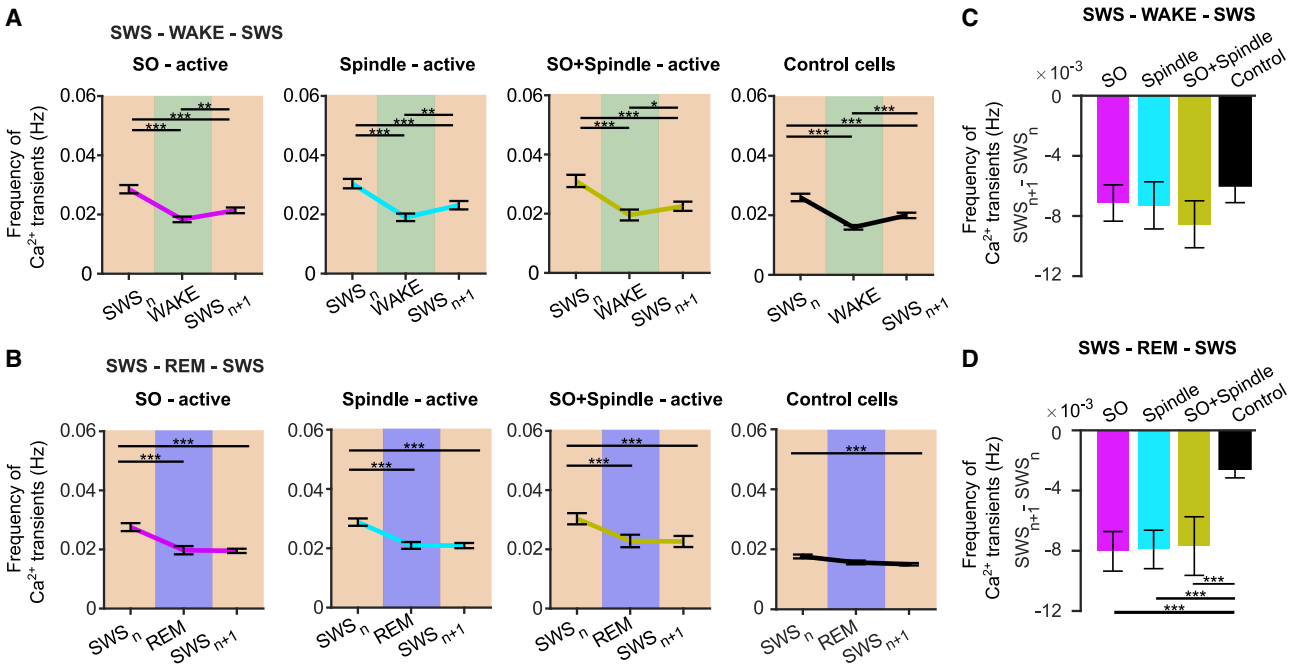

Figure 7. Cells active during SOs and spindles show the strongest downregulation of Ca^{2+} transient frequency across SWS epochs interleaved by REM epochs

(A and B) Mean ± SEM Ca^{2+} transient frequency of SO-active, Spindle-active, SO + Spindle-active, and control cells during two consecutive epochs of SWS (SWS_n and SWS_{n+1}) interleaved by wake (A) and REM (B) epochs. $^*p \leq 0.05$, $^{**}p < 0.01$, $^{***}p < 0.001$, LMM followed by the Wilcoxon signed-rank test.

(C and D) Mean ± SEM changes in Ca^{2+} transient frequency between SWS_n and SWS_{n+1} epochs interleaved by wake (C) and REM (D) epochs for SO-active (n = 100 triplets), spindle-active (n = 100 triplets), SO + Spindle-active (n = 76 triplets), and control cells (n = 100 triplets). LMM followed by the Mann-Whitney U test. $^{***}p < 0.001$.

See also Figures S6 and S7.

(4) Sleep spindle events themselves were accompanied by a rapid reduction in both the fraction of active cells and the mean amplitude of Ca^{2+} transients within seconds after their onset. Together, these findings suggest that hippocampal network activity is not generally downregulated within individual sleep epochs but instead undergoes a gradual activity-dependent modulation across successive SWS epochs—a regulatory process that is mediated via spindle and REM-related mechanisms.

We found that compared with wakefulness, sleep is associated with enhanced CA1 neuronal activity, with the number of active cells reaching a maximum during REM sleep. Although REM sleep showed the highest cell recruitment and the largest amplitudes of Ca^{2+} transients, network dynamics were more desynchronized than in other states. By contrast, during SWS, the relatively low frequency of Ca^{2+} transients was accompanied by stronger co-activation, consistent with the idea that SOs drive synchronized neuronal activity. Of note, the relatively low activation during wakefulness might be owed to the fact that we focused on periods of "quiet" wakefulness occurring between sleep bouts, and the mice, being highly habituated to the experimental setup, were not engaging in any particular task. Our observation concurs with previous electrophysiological findings[38] showing that in CA1 the majority of neurons are silent during wakefulness. The increase in activated cell numbers reaching a maximum during REM sleep—in conjunction with a faster recruitment of cells and a higher amplitude of Ca^{2+} transients during REM sleep than SWS—might reflect specific network properties in the hippocampus, where the ratio of inhibitory to excitatory cells is rather low, compared with most neocortical networks.[39,40] In the neocortex, network activity during REM sleep is governed by the predominant activity of inhibitory interneurons (parvalbumin-positive basket cells), producing a general suppression of network activity.[41–43] Whether REM sleep is characterized by a similar preferential upregulation of inhibitory activity in hippocampal networks cannot be answered based on the present data. The increase in Ca^{2+} transient amplitude occurring in combination with a relative increase in frequency of transients during REM sleep in comparison with SWS might indeed reflect the presence of a more burst-like firing pattern during REM sleep, as it can originate from an enhanced recurrent inhibition.[44]

Unexpectedly, we did not find any decrease in hippocampal Ca^{2+} signaling within epochs of either SWS or REM sleep for the total population of pyramidal cells. This finding contrasts with results obtained from Ca^{2+} imaging of neocortical circuits, which demonstrated a reduction in Ca^{2+} signaling of layer 2/3 pyramidal cells during SWS and REM sleep.[16] At first glance, this finding, moreover, appears to challenge the view, as put forward by the SHY, that the widespread synaptic downregulation during sleep extends to hippocampal networks. In fact, this view is well supported by studies showing reduced expression of glutamatergic AMPA receptors in the hippocampus following sleep compared with wake periods.[45] However, it is important to

note that our imaging approach, which captures ongoing Ca^{2+} transients, primarily reflects network excitability rather than providing a direct measure of synaptic strength or connectivity. Therefore, it may well be that sleep-dependent synaptic downscaling in CA1 during sleep was masked by widespread release of inhibition in these networks. Accordingly, these seemingly discrepant findings might be resolved in a combined assessment of activity in excitatory and inhibitory networks.

Notably, we did not observe a downregulation of Ca^{2+} transient frequency and amplitude for the overall hippocampal cell population across successive SWS epochs, as previously reported using electrophysiological recordings.[46–48] This discrepancy likely reflects methodological differences between Ca^{2+} imaging and electrophysiological recordings of neuronal spikes as used in those previous studies. Typically, such electrophysiological approaches apply a firing rate threshold,[46] thereby excluding low-activity and silent neurons, whereas our imaging approach included the total recorded cell population. In addition, electrophysiological recordings primarily capture neurons with ongoing spiking, whereas Ca^{2+} imaging emphasizes burst-related activity, providing altogether a complementary but not identical view on network activity. Indeed, when we restricted our analysis to subpopulations that showed at least one Ca^{2+} transient during the SWS_n epoch (Figure 7), we observed the expected decrease in transient frequency during the subsequent SWS_{n+1} epoch. Ca^{2+} transient frequency also decreased across successive SWS epochs for cells showing enhanced activity during SOs and spindles. Together, these findings match well with electrophysiological findings showing that hippocampal spindles and ripples predict changes in neuronal activity between consecutive SWS epochs,[47] and they extend these observations to SO and SO + Spindle events. Overall, the observed dynamics suggest a downregulation of activity across extended sleep bouts, selectively affecting cells engaged in memory processing during SWS.[2,3]

We found that the extent of downregulation across SWS epochs strongly depends on the duration of the preceding SWS epoch as well as on spindle density during this epoch. Indeed, the duration of the initial SWS epoch was the only negative predictor of downregulation, i.e., the longer the initial SWS epoch was, the less downregulation of Ca^{2+} signaling occurred across the two consecutive epochs, which points to the importance of memory processing during SWS that counters, and in this way determines, the degree of subsequent downregulation of activity in the respective cell subpopulations.[49]

Spindle activity during the initial SWS epoch, on the other hand, was a positive predictor of downregulation of activity across consecutive SWS epochs, i.e., the higher the spindle density was during the initial SWS epoch, the more network activity was downregulated during the succeeding SWS epoch. Moreover, acute spindle events were directly followed by a decrease in CA1 network activity, which likewise points to a role of spindles in downregulating hippocampal CA1 activity. Consistent with this view, in neocortical circuits spindles appear to regulate plasticity primarily through activating inhibitory (parvalbumin-positive) basket cells while simultaneously reducing dendritic inhibition from somatostatin-positive cells.[16] Inhibitory cells may likewise convey the effects of thalamic spindles spreading to hippocampal networks. Ripples, which in hippocampal networks tend to nest into the troughs of the spindle oscillation,[22] may additionally contribute. Indeed, ripples play a 2-fold role in plasticity, on the one hand promoting the downscaling of hippocampal synapses.[25] On the other hand, they contribute to stabilizing hippocampal memory representations by coordinating memory replay.[50–52] One might speculate that the nesting of ripples into the sequence of spindle oscillations, beyond supporting the hippocampal-to-neocortical transmission of reactivated memory information,[21,53] simultaneously augments the synaptic downscaling effect of these ripples.[25] However, as we did not record hippocampal local field potentials, this study cannot address this issue.

Importantly, we found that the downregulation of cells active during SOs and spindles was most robust across consecutive SWS epochs that were separated by an intermittent REM sleep epoch. Moreover, these cells tended to upregulate activity in the course of REM epochs, pointing to a specific contribution of this sleep stage to memory processing. In combination, these findings are consistent with a scenario where sleep spindle-associated cell activity during SWS initiates processes shaping the downregulation of hippocampal networks during subsequent REM sleep, an idea also in line with evidence indicating that spindle density during an SWS epoch predicts the onset of subsequent REM sleep.[54] Yet this idea, as well as the question of to what extent REM sleep-related downregulation eventually manifests in structural changes in hippocampal networks, as observed in cortical synapses,[32,55] warrants further investigation.

Our study has several limitations, such as the missing recordings of inhibitory interneuron activity as well as active manipulation of memory, which hampers straightforward conclusions as to the extent to which the cells active during SOs and spindles are critical for memory processing. Additionally, due to technical challenges (space on the animal's head and weight of the mounted devices), hippocampal LFPs were not recorded. Therefore, we did not examine ripple activity, and thus our observations of spindle- and SO-associated cell activity are not directly linked to canonical hippocampal memory signatures. Nevertheless, our data reveal distinct sleep-dependent patterns of activation for these cells and the total population of CA1 pyramidal neurons, patterns that clearly differ from the dynamics found in neocortical circuits.[33] Unlike in neocortical networks, where spindle-active pyramidal cells upregulated their activity within SWS epochs, we did not observe such upregulation for hippocampal pyramidal cells but, instead, signs of a spindle-initiated downregulation across SWS epochs that reaches full expression with intermittent REM sleep. Although our study identifies spindles as a potential key factor in the downregulation of hippocampal activity, the causal role of spindles in this process needs to be scrutinized in the future. Determining whether spindles are necessary or sufficient for hippocampal renormalization requires targeted manipulations, such as spindle-specific optogenetic interventions, which represent important directions for future research.

RESOURCE AVAILABILITY

Lead contact

Requests for further information and resources should be directed to and will be fulfilled by the lead contact, Olga Garaschuk (olga.garaschuk@uni-tuebingen.de).

Materials availability

This study did not generate any new, unique reagents.

Data and code availability

- All data reported in this paper will be shared by the lead contact upon request.
- Key analysis code is available at: Zenodo: https://doi.org/10.5281/zenodo.18714655.
- The datasets generated during this study and any additional information required to reanalyze the data reported in this paper are available upon request from the lead contact.

ACKNOWLEDGMENTS

We thank E. Zirdum and K. Schmidt for technical assistance, F. Kamari for help with data analysis, and S. Nevelchuk for the ECG subtraction algorithm. This work was supported by grants from the Deutsche Forschungsgemeinschaft (FOR 5434, GA654/16-1, GA654/18-1, and BO854/17-1) to O.G. and J.B.; from the European Research Council to J.B. (ERC AdG 883098 SleepBalance); from the German Federal Ministry of Education and Research (BMBF) to the German Center for Diabetes Research (DZD e.V.); and from the Hertie Foundation, Network for Excellence in Clinical Neuroscience, to N.N. The funders had no role in the study design, data collection and analysis, the decision to publish, or preparation of the manuscript.

AUTHOR CONTRIBUTIONS

Conceptualization, N.N., J.B., and O.G.; methodology, Y.K. and N.N.; investigation, D.M.P. and Y.K.; formal analysis, N.M., D.M.P., Y.K., and N.N.; writing – original draft, D.M.P., O.G., and N.N.; writing – review & editing, N.N., O.G., and J.B.; visualization, D.M.P., N.M., O.G., and N.N.; funding acquisition, O.G., J.B., and N.N.; supervision, J.B. and O.G.

DECLARATION OF INTERESTS

The authors declare no competing interests.

STAR★METHODS

Detailed methods are provided in the online version of this paper and include the following:

- KEY RESOURCES TABLE
- EXPERIMENTAL MODEL AND STUDY PARTICIPANT DETAILS
- METHOD DETAILS
  - Surgery
  - Training for head fixation
  - EEG and EMG recordings
  - Detection of slow oscillations and sleep spindles
  - Two-photon imaging
  - Two-photon image analyses
  - Detection of SO-active, Spindle-active, and SO+Spindle-active cells
- QUANTIFICATION AND STATISTICAL ANALYSIS

SUPPLEMENTAL INFORMATION

Supplemental information can be found online at https://doi.org/10.1016/j.cub.2026.01.075.

Received: July 31, 2025
Revised: December 14, 2025
Accepted: January 30, 2026
Published: February 27, 2026

REFERENCES

1. Tononi, G., and Cirelli, C. (2014). Sleep and the price of plasticity: from synaptic and cellular homeostasis to memory consolidation and integration. Neuron *81*, 12–34. https://doi.org/10.1016/j.neuron.2013.12.025.
2. Brodt, S., Inostroza, M., Niethard, N., and Born, J. (2023). Sleep – A brain-state serving systems memory consolidation. Neuron *111*, 1050–1075. https://doi.org/10.1016/j.neuron.2023.03.005.
3. Klinzing, J.G., Niethard, N., and Born, J. (2019). Mechanisms of systems memory consolidation during sleep. Nat. Neurosci. *22*, 1598–1610. https://doi.org/10.1038/s41593-019-0467-3.
4. Tononi, G., and Cirelli, C. (2020). Sleep and synaptic down-selection. Eur. J. Neurosci. *51*, 413–421. https://doi.org/10.1111/ejn.14335.
5. Buzsáki, G. (1996). The hippocampo-neocortical dialogue. Cereb. Cortex *6*, 81–92. https://doi.org/10.1093/cercor/6.2.81.
6. Sirota, A., Csicsvari, J., Buhl, D., and Buzsáki, G. (2003). Communication between neocortex and hippocampus during sleep in rodents. Proc. Natl. Acad. Sci. USA *100*, 2065–2069. https://doi.org/10.1073/pnas.0437938100.
7. Diekelmann, S., and Born, J. (2010). The memory function of sleep. Nat. Rev. Neurosci. *11*, 114–126. https://doi.org/10.1038/nrn2762.
8. Sawangjit, A., Oyanedel, C.N., Niethard, N., Salazar, C., Born, J., and Inostroza, M. (2018). The hippocampus is crucial for forming non-hippocampal long-term memory during sleep. Nature *564*, 109–113. https://doi.org/10.1038/s41586-018-0716-8.
9. Steriade, M. (2003). The corticothalamic system in sleep. Front. Biosci. *8*, d878–d899. https://doi.org/10.2741/1043.
10. Fernandez, L.M.J., and Lüthi, A. (2020). Sleep spindles: Mechanisms and functions. Physiol. Rev. *100*, 805–868. https://doi.org/10.1152/physrev.00042.2018.
11. Liu, A.A., Henin, S., Abbaspoor, S., Bragin, A., Buffalo, E.A., Farrell, J.S., Foster, D.J., Frank, L.M., Gedankien, T., Gotman, J., et al. (2022). A consensus statement on detection of hippocampal sharp wave ripples and differentiation from other fast oscillations. Nat. Commun. *13*, 6000. https://doi.org/10.1038/s41467-022-33536-x.
12. Steriade, M., McCormick, D.A., and Sejnowski, T.J. (1993). Thalamocortical oscillations in the sleeping and aroused brain. Science *262*, 679–685. https://doi.org/10.1126/science.8235588.
13. De Gennaro, L., and Ferrara, M. (2003). Sleep spindles: an overview. Sleep Med. Rev. *7*, 423–440. https://doi.org/10.1053/smrv.2002.0252.
14. Mölle, M., and Born, J. (2011). Slow oscillations orchestrating fast oscillations and memory consolidation. Prog. Brain Res. *193*, 93–110. https://doi.org/10.1016/B978-0-444-53839-0.00007-7.
15. Chauvette, S., Seigneur, J., and Timofeev, I. (2012). Sleep oscillations in the thalamocortical system induce long-term neuronal plasticity. Neuron *75*, 1105–1113. https://doi.org/10.1016/j.neuron.2012.08.034.
16. Niethard, N., Ngo, H.V.V., Ehrlich, I., and Born, J. (2018). Cortical circuit activity underlying sleep slow oscillations and spindles. Proc. Natl. Acad. Sci. USA *115*, E9220–E9229. https://doi.org/10.1073/pnas.1805517115.
17. Peyrache, A., and Seibt, J. (2020). A mechanism for learning with sleep spindles. Philos. Trans. R. Soc. Lond. B Biol. Sci. *375*, 20190230. https://doi.org/10.1098/rstb.2019.0230.
18. Clemens, Z., Mölle, M., Eröss, L., Jakus, R., Rásonyi, G., Halász, P., and Born, J. (2011). Fine-tuned coupling between human parahippocampal ripples and sleep spindles. Eur. J. Neurosci. *33*, 511–520. https://doi.org/10.1111/j.1460-9568.2010.07505.x.
19. Clemens, Z., Mölle, M., Eross, L., Barsi, P., Halász, P., and Born, J. (2007). Temporal coupling of parahippocampal ripples, sleep spindles and slow oscillations in humans. Brain *130*, 2868–2878. https://doi.org/10.1093/brain/awm146.
20. Staresina, B.P., Bergmann, T.O., Bonnefond, M., van der Meij, R., Jensen, O., Deuker, L., Elger, C.E., Axmacher, N., and Fell, J. (2015). Hierarchical nesting of slow oscillations, spindles and ripples in the human hippocampus during sleep. Nat. Neurosci. *18*, 1679–1686. https://doi.org/10.1038/nn.4119.

21. Oyanedel, C.N., Durán, E., Niethard, N., Inostroza, M., and Born, J. (2020). Temporal associations between sleep slow oscillations, spindles and ripples. Eur. J. Neurosci. *52*, 4762–4778. https://doi.org/10.1111/ejn.14906.

22. Latchoumane, C.V., Ngo, H.-V.V., Born, J., and Shin, H.-S. (2017). Thalamic spindles promote memory formation during sleep through triple phase-locking of cortical, thalamic, and hippocampal rhythms. Neuron *95*, 424–435.e6. https://doi.org/10.1016/j.neuron.2017.06.025.

23. Varela, C., Kumar, S., Yang, J.Y., and Wilson, M.A. (2014). Anatomical substrates for direct interactions between hippocampus, medial prefrontal cortex, and the thalamic nucleus reuniens. Brain Struct. Funct. *219*, 911–929. https://doi.org/10.1007/s00429-013-0543-5.

24. Cirelli, C., and Tononi, G. (2020). Effects of sleep and waking on the synaptic ultrastructure. Philos. Trans. R. Soc. Lond. B Biol. Sci. *375*, 20190235. https://doi.org/10.1098/rstb.2019.0235.

25. Norimoto, H., Makino, K., Gao, M., Shikano, Y., Okamoto, K., Ishikawa, T., Sasaki, T., Hioki, H., Fujisawa, S., and Ikegaya, Y. (2018). Hippocampal ripples down-regulate synapses. Science *359*, 1524–1527. https://doi.org/10.1126/science.aao0702.

26. Puentes-Mestril, C., and Aton, S.J. (2017). Linking network activity to synaptic plasticity during sleep: hypotheses and recent data. Front. Neural Circuits *11*, 61. https://doi.org/10.3389/fncir.2017.00061.

27. Niethard, N., Burgalossi, A., and Born, J. (2017). Plasticity during sleep is linked to specific regulation of cortical circuit activity. Front. Neural Circuits *11*, 65. https://doi.org/10.3389/fncir.2017.00065.

28. Olcese, U., Esser, S.K., and Tononi, G. (2010). Sleep and synaptic renormalization: a computational study. J. Neurophysiol. *104*, 3476–3493. https://doi.org/10.1152/jn.00593.2010.

29. Liu, J., Niethard, N., Lun, Y., Dimitrov, S., Ehrlich, I., Born, J., and Hallschmid, M. (2024). Slow-wave sleep drives sleep-dependent renormalization of synaptic AMPA receptor levels in the hypothalamus. PLoS Biol. *22*, e3002768. https://doi.org/10.1371/journal.pbio.3002768.

30. Squarcio, F., Tononi, G., and Cirelli, C. (2024). Effects of non-rapid eye movement sleep on the cortical synaptic expression of GluA1-containing AMPA receptors. Eur. J. Neurosci. *60*, 3961–3972. https://doi.org/10.1111/ejn.16460.

31. Watson, B.O., Levenstein, D., Greene, J.P., Gelinas, J.N., and Buzsáki, G. (2016). Network homeostasis and state dynamics of neocortical sleep. Neuron *90*, 839–852. https://doi.org/10.1016/j.neuron.2016.03.036.

32. Li, W., Ma, L., Yang, G., and Gan, W.-B. (2017). REM sleep selectively prunes and maintains new synapses in development and learning. Nat. Neurosci. *20*, 427–437. https://doi.org/10.1038/nn.4479.

33. Niethard, N., Brodt, S., and Born, J. (2021). Cell-type-specific dynamics of calcium activity in cortical circuits over the course of slow-wave sleep and rapid eye movement sleep. J. Neurosci. *41*, 4212–4222. https://doi.org/10.1523/JNEUROSCI.1957-20.2021.

34. Bojarskaite, L., Bjørnstad, D.M., Pettersen, K.H., Cunen, C., Hermansen, G.H., Åbjørsbråten, K.S., Chambers, A.R., Sprengel, R., Vervaeke, K., Tang, W., et al. (2020). Astrocytic Ca^{2+} signaling is reduced during sleep and is involved in the regulation of slow wave sleep. Nat. Commun. *11*, 3240. https://doi.org/10.1038/s41467-020-17062-2.

35. Binder, S., Mölle, M., Lippert, M., Bruder, R., Aksamaz, S., Ohl, F., Wiegert, J.S., and Marshall, L. (2019). Monosynaptic hippocampal-prefrontal projections contribute to spatial memory consolidation in mice. J. Neurosci. *39*, 6978–6991. https://doi.org/10.1523/JNEUROSCI.2158-18.2019.

36. Dana, H., Sun, Y., Mohar, B., Hulse, B.K., Kerlin, A.M., Hasseman, J.P., Tsegaye, G., Tsang, A., Wong, A., Patel, R., et al. (2019). High-performance calcium sensors for imaging activity in neuronal populations and microcompartments. Nat. Methods *16*, 649–657. https://doi.org/10.1038/s41592-019-0435-6.

37. Vyazovskiy, V.V.V., Olcese, U., Lazimy, Y.M., Faraguna, U., Esser, S.K., Williams, J.C., Cirelli, C., and Tononi, G. (2009). Cortical firing and sleep homeostasis. Neuron *63*, 865–878. https://doi.org/10.1016/j.neuron.2009.08.024.

38. Karlsson, M.P., and Frank, L.M. (2008). Network dynamics underlying the formation of sparse, informative representations in the hippocampus. J. Neurosci. *28*, 14271–14281. https://doi.org/10.1523/JNEUROSCI.4261-08.2008.

39. Jinno, S., and Kosaka, T. (2006). Cellular architecture of the mouse hippocampus: A quantitative aspect of chemically defined GABAergic neurons with stereology. Neurosci. Res. *56*, 229–245. https://doi.org/10.1016/j.neures.2006.07.007.

40. Ahmed, O.J., and Mehta, M.R. (2009). The hippocampal rate code: anatomy, physiology and theory. Trends Neurosci. *32*, 329–338. https://doi.org/10.1016/j.tins.2009.01.009.

41. Niethard, N., Hasegawa, M., Itokazu, T., Oyanedel, C.N., Born, J., and Sato, T.R. (2016). Sleep-stage-specific regulation of cortical excitation and inhibition. Curr. Biol. *26*, 2739–2749. https://doi.org/10.1016/j.cub.2016.08.035.

42. Aime, M., Calcini, N., Borsa, M., Campelo, T., Rusterholz, T., Sattin, A., Fellin, T., and Adamantidis, A. (2022). Paradoxical somatodendritic decoupling supports cortical plasticity during REM sleep. Science *376*, 724–730. https://doi.org/10.1126/science.abk2734.

43. Lendner, J.D., Niethard, N., Mander, B.A., van Schalkwijk, F.J., Schuh-Hofer, S., Schmidt, H., Knight, R.T., Born, J., Walker, M.P., Lin, J.J., et al. (2023). Human REM sleep recalibrates neural activity in support of memory formation. Sci. Adv. *9*, eadj1895. https://doi.org/10.1126/sciadv.adj1895.

44. Zhou, H., Neville, K.R., Goldstein, N., Kabu, S., Kausar, N., Ye, R., Nguyen, T.T., Gelwan, N., Hyman, B.T., and Gomperts, S.N. (2019). Cholinergic modulation of hippocampal calcium activity across the sleep-wake cycle. eLife *8*, e39777. https://doi.org/10.7554/eLife.39777.

45. Vyazovskiy, V.V., Cirelli, C., Pfister-Genskow, M., Faraguna, U., and Tononi, G. (2008). Molecular and electrophysiological evidence for net synaptic potentiation in wake and depression in sleep. Nat. Neurosci. *11*, 200–208. https://doi.org/10.1038/nn2035.

46. Grosmark, A.D., Mizuseki, K., Pastalkova, E., Diba, K., and Buzsáki, G. (2012). REM sleep reorganizes hippocampal excitability. Neuron *75*, 1001–1007. https://doi.org/10.1016/j.neuron.2012.08.015.

47. Miyawaki, H., and Diba, K. (2016). Regulation of hippocampal firing by network oscillations during sleep. Curr. Biol. *26*, 893–902. https://doi.org/10.1016/j.cub.2016.02.024.

48. Miyawaki, H., Watson, B.O., and Diba, K. (2019). Neuronal firing rates diverge during REM and homogenize during non-REM. Sci. Rep. *9*, 689. https://doi.org/10.1038/s41598-018-36710-8.

49. Miyamoto, D., Marshall, W., Tononi, G., and Cirelli, C. (2021). Net decrease in spine-surface GluA1-containing AMPA receptors after post-learning sleep in the adult mouse cortex. Nat. Commun. *12*, 2881. https://doi.org/10.1038/s41467-021-23156-2.

50. Fernández-Ruiz, A., Oliva, A., Fermino de Oliveira, E., Rocha-Almeida, F., Tingley, D., and Buzsáki, G. (2019). Long-duration hippocampal sharp wave ripples improve memory. Science *364*, 1082–1086. https://doi.org/10.1126/science.aax0758.

51. Oliva, A., Fernández-Ruiz, A., Leroy, F., and Siegelbaum, S.A. (2020). Hippocampal CA2 sharp-wave ripples reactivate and promote social memory. Nature *587*, 264–269. https://doi.org/10.1038/s41586-020-2758-y.

52. Gridchyn, I., Schoenenberger, P., O'Neill, J., and Csicsvari, J. (2020). Assembly-specific disruption of hippocampal replay leads to selective memory deficit. Neuron *106*, 291–300.e6. https://doi.org/10.1016/j.neuron.2020.01.021.

53. Mölle, M., Eschenko, O., Gais, S., Sara, S.J., and Born, J. (2009). The influence of learning on sleep slow oscillations and associated spindles and ripples in humans and rats. Eur. J. Neurosci. *29*, 1071–1081. https://doi.org/10.1111/j.1460-9568.2009.06654.x.

54. Bandarabadi, M., Herrera, C.G., Gent, T.C., Bassetti, C., Schindler, K., and Adamantidis, A.R. (2020). A role for spindles in the onset of rapid eye movement sleep. Nat. Commun. *11*, 1–12.

55. Yang, G., Lai, C.S.W., Cichon, J., Ma, L., Li, W., and Gan, W.-B. (2014). Sleep promotes branch-specific formation of dendritic spines after learning. Science *344*, 1173–1178. https://doi.org/10.1126/science.1249098.

56. Dombeck, D.A., Harvey, C.D., Tian, L., Looger, L.L., and Tank, D.W. (2010). Functional imaging of hippocampal place cells at cellular resolution during virtual navigation. Nat. Neurosci. *13*, 1433–1440. https://doi.org/10.1038/nn.2648.

57. Pachitariu, M., Stringer, C., Dipoppa, M., Schröder, S., Rossi, L.F., Dalgleish, H., Carandini, M., and Harris, K. (2016). Suite2p: beyond 10,000 neurons with standard two-photon microscopy. Preprint at bioRxiv. https://doi.org/10.1101/061507.

STAR★METHODS

KEY RESOURCES TABLE

REAGENT or RESOURCE	SOURCE	IDENTIFIER
Bacterial and viral strains		
AAV-syn-jGCaMP7b-WPRE	Addgene	RRID:Addgene_104489
scAAV-DJ/8/2-mDlx-HBB-chI-mRuby3-SV40p(A)	Viral Vector Facility of the Zürich University	v242-DJ/8; https://www.vvf.uzh.ch/en.html
Experimental models: Organisms/strains		
C57BL6/N	Charles River	RRID: MGI:7466658
Software and algorithms		
Suite2P	Github	RRID: SCR_016434
MATLAB 2024b	Mathworks	RRID: SCR_001622
Spike2	Cambridge Electronic Design	RRID: SCR_000903

EXPERIMENTAL MODEL AND STUDY PARTICIPANT DETAILS

Seven 5-6 months old male C57BL6/N mice were kept in pathogen-free conditions at 22 °C, 60% air humidity, 12/12-hour light/dark-cycle (lights on at 7.00 a.m.) with ad libitum access to food and water. All recordings started during the first hour of the light phase. All experimental procedures were in accordance with the Directive 2010/63/EU of the European Parliament and the Council of the European Union and were approved by the state government of Baden-Württemberg, Germany.

METHOD DETAILS

Surgery

Virus injection: all surgical procedures were conducted on a stereotactic apparatus under 3-component anesthesia (Fentanyl 0,05 mg/kg KGW, Midazolam 5,0 mg/kg BW, Medetomidine 0,5 mg/kg BW, injection volume 0,1 ml pro 10 g BW) and local analgesia using 2% lidocaine. During all steps of surgery, the animals were kept on a warming plate, with the body temperature continuously monitored and kept at 37 °C. Using a dental drill (NSK, Eschborn, Germany), a small (Ø 0.5-1 mm) craniotomy was performed above the right hippocampus (-1.8 mm anterior-posterior (AP), -1.5 mm medial-lateral (ML) from bregma) and$\sim$ 600 nL of viral solution (either AAV-syn-jGCaMP7b-WPRE (product #104489, Addgene, USA), titer $\geq 1\times10^{12}$ vg/mL or a mixture of the above virus with a scAAV-DJ/8/2-mDlx-HBB-chI-mRuby3-SV40p(A) virus (Viral Vector Facility of the Zürich University), titer $\geq$6.2x10^{12} vg/mL) was injected 1.5 mm below the dura.[56] The mice were kept on a heated plate until full recovery from anesthesia. Postoperative care included an analgesic dose of carprofen (5 μg/g BW).

Implantation of the cranial window and EEG/EMG electrodes: Cortical aspiration was performed 10 days after the viral injection according to a published protocol.[56] A craniotomy (Ø 3 mm) was centered around the virus injection spot. Aspiration was used to slowly remove the cortex within the craniotomy. The removal was accomplished very slowly (within 6-7 min) with aspiration of $\sim$50−100 μm of tissue at a time, followed by repeated irrigation with saline containing (in mM) 125 NaCl, 4 KCl, 1 $KH2PO_4$, 1 $MgSO_4$, 2.2 $CaCl_2$, and 20 HEPES, until any bleeding stopped and the external capsule was exposed. The topmost layers of the external capsule were gently peeled away with a swab soaked in saline until the surface of the hippocampus looked translucent. The imaging window, consisting of a glass coverslip (Ø 3 mm) glued to the bottom of a 1.5 mm long stainless-steel cannula, was inserted into the craniotomy such that the glass was in direct contact with the hippocampal surface. The implant was secured with cyanoacrylate glue and blue light-cured dental cement. Subsequently, three holes were drilled in the skull of the contralateral hemisphere to implant the EEG electrodes (frontal: +1.5 mm AP, 1.5 mm ML; parietal: -1.5 mm AP, 2.5 mm ML). The reference electrode was implanted above the cerebellum. The EEG electrodes were inserted into the holes in direct contact with the dura mater and fixed to the skull with dental cement. Two stainless-steel wires (Science Products GmbH, Hofheim am Taunus) were inserted in the nuchal muscles for EMG recordings. A custom-made titanium holder was centered on the cranial window and fixed to the skull with dental cement. The mice were placed on a heating plate to recover. Postoperative care included an analgesic dose of carprofen (5 μg/g BW) for 3 days subcutaneously and the antibiotic Enrofloxacin in drinking water (final concentration 0.025%) for consecutive 10 days. Mice were allowed to recover for at least 2 weeks and were subsequently examined for window clarity. After surgery, the mice were single-housed, again on a 12/12 h light/dark cycle with food and water available *ad libitum*.

Training for head fixation

Every animal was subjected to an individual training protocol consisting of several sequential steps: (i) gentle handling inside their home cages (∼ one week), (ii) habituation to the experimental set-up, including head fixation (at least two weeks). Each habituation session consisted of gentle handling followed by a >20-min period of free exploration of the setup. Thereafter, the mice were head-fixed under the microscope on a custom-made linear treadmill for an increasing time interval (1 min, 10 min, 30 min, 60 min). Each fixation was followed by a 5-min-long rest period. After this initial habituation phase, the animals were head-fixed for longer periods (2-3 hours), mimicking the imaging sessions. The training sessions and imaging experiments (see below) started within one hour after lights on.

EEG and EMG recordings

The electrophysiological signals were amplified, filtered (EEG: 0.01-300 Hz; EMG: 30-300 Hz), and sampled at 1 kHz using a differential low-noise amplifier (AD Instruments, Ltd, Oxford). Signals were divided into 10-s-long time bins, which were manually scored to discriminate the different sleep stages (wakefulness, SWS, and REM sleep). Wakefulness was identified by rapid, low-amplitude activity accompanied by increased EMG tone. SWS was distinguished by prevalent high-amplitude delta activity (<4.0 Hz), the presence of sleep spindles (11-16 Hz), and reduced EMG activity, and REM sleep by the prevalence of theta activity (5.0-10.0 Hz), muscle twitches, and minimal EMG activity. Sleep scoring was supported by custom routines in Spike2 software (CED, Cambridge, UK).

For display purposes (Figures 1 and S1–S4), the ECG artefacts were removed from the EMG signals using a PCA-based pattern subtraction algorithm. To do so, the QRS complexes were detected in the EMG signal based on their stereotypic shape and amplitude, and fixed-length time frames were placed around each R-peak. Subsequently, each framed segment was projected into a PCA space. Since ECG artifacts are similar across heartbeats while EMG activity is stochastic, PCA captures the time course of the ECG artifact in the 1st principal component. Subsequently, the EMG signal was reconstructed without the 1st principal component.

Detection of slow oscillations and sleep spindles

The algorithms for the detection of sleep spindles and SOs were adopted from previous studies.[33] Sleep spindles were detected in EEG recordings, band-pass filtered between 7-15 Hz, and rectified. The absolute values of the Hilbert-transformed filtered signal were used to yield the envelope for the frequency band of interest. A spindle event was identified whenever the envelope exceeded a threshold of 1.5 standard deviations (SD) of the filtered signal during SWS for 0.5-3 s. The onset and end of the spindle event were marked by the positive and negative crossings of the threshold, respectively. For the detection of SOs, the signals were band-pass filtered between 0.1-4 Hz. All positive-to-negative zero-crossings were marked. The event was marked as a SO if the duration between two succeeding positive-to-negative crossings was between 0.4 and 2 s and if the minimum-to-maximum amplitude was > 66.6% of the average of the respective amplitude values across the entire recording session. When the onset of a spindle occurred in the interval between the negative half-wave peak and the positive half-wave peak of an SO, it was identified as an SO+Spindle event.[16]

Two-photon imaging

Mice were placed on a custom-made linear treadmill and head-fixed under a two-photon resonant scanner microscope (FemtoSmart-Dual, Femtonics Ltd, Budapest) with a 256 μm x 256 μm imaging frame and a frame rate of 30 Hz. GCaMP7b was excited at 930 nm with a femtosecond-pulsed two-photon laser (Mai Tai DeepSee, Spectra-Physics). Images of the CA1 pyramidal cell layer (containing 150-250 cell somata) were acquired with a water-immersion objective (Nikon 40x, 0.8 NA, Nikon, Tokyo, Japan) from the stratum pyramidale at a depth of 100 μm below the hippocampal surface, thus targeting deep (calbindin-negative) CA1 pyramidal cells.

Two-photon image analyses

Registration of the acquired time series was performed with Suite2p.[57] Regions of interest (ROIs) were manually drawn over cell somata, and the individual fluorescence traces were calculated as the average pixel intensity for each ROI. Slow baseline fluctuations were removed from the fluorescent traces using the 8th percentile threshold in a rolling window of 60 s.[56] The baseline F_0 was calculated by measuring the 10th percentile of the corrected trace and was used to calculate relative changes in fluorescence ($\Delta F/F$) for individual neurons. The $\Delta F/F$ changes were counted as Ca^{2+} transients when the amplitude of the signal was higher than the tenfold SD of the corresponding baseline noise. The baseline noise was estimated using a wavelet-based approach.[56]

Detection of SO-active, Spindle-active, and SO+Spindle-active cells

For each cell and each epoch, we calculated the difference between the mean frequency of Ca^{2+} transients during a given type of oscillatory events (i.e., SOs, Spindles or SO+Spindles) and the remaining period of the respective SWS epoch. All cells with a positive difference were defined as SO-, spindle-, or SO+Spindle-active cells, respectively, whereas the cells with a negative difference were considered as control cells.

QUANTIFICATION AND STATISTICAL ANALYSIS

All statistical analyses were conducted using MATLAB R2024b (MathWorks, USA). To evaluate the effects of brain state on changes in Ca^{2+} activity across sleep epochs, we employed linear mixed-effects models (LMMs) using the fitlme function from the Statistics and Machine Learning Toolbox. For analyses involving changes across the three thirds of a sleep epoch, we compiled a dataset containing animal identity, Ca^{2+} transient frequency/amplitude, brain state (wake, SWS, REM), and epoch segment (1^{st}, 2^{nd}, 3^{rd} third). We first fit a full model including fixed effects for brain state and epoch third, as well as their interaction, with a random intercept for animal: (Ca^{2+} signaling $\sim$ Brain State * Third + (1|Animal)).

Significance of interaction and main effects was assessed using likelihood ratio tests (Matlab function 'compare'). If the interaction term was not significant ($p \geq 0.05$), we used a reduced model: (Ca^{2+} signaling $\sim$ Brain State + Third + (1|Animal)). We then tested for main effects by sequentially removing from the model one factor at a time (e.g., Ca^{2+} signaling $\sim$ Subpopulation + (1|Animal) or Ca^{2+} signaling $\sim$ Brain State + (1|Animal)). Similar LMMs were used to compare Ca^{2+} transient frequency/amplitude across sequential sleep triplets—SWS_n–REM–SWS_{n+1} and SWS_n–Wake–SWS_{n+1}—using the following model: (Ca^{2+} signaling $\sim$ Intervening-State * Triplet + (1|Animal)) where Triplet denotes the position in the sequence (SWS_n REM/Wake SWS_{n+1}), and Intervening State refers to the state type (REM or wake) between the two SWS epochs.

For analyses involving activity across cell subpopulations (SO-active, spindle-active, SO+Spindle-active, and control), we used analogous models that included Subpopulation as a fixed factor: (Ca^{2+} signaling $\sim$ Brain State * Subpopulation + (1|Animal)). Post hoc comparisons were performed using two-sided Wilcoxon rank-sum tests (for independent samples) and two-sided Wilcoxon signed-rank tests (for paired samples). Results were considered statistically significant at $p < 0.05$. Spearman correlation was used for all correlation analyses.